Induced pluripotent stem cells derived from mouse models of lysosomal storage disorders

Xing-Li Meng[a,b,1], Jin-Song Shen[a,b,1,2], Shiho Kawagoe[b], Toya Ohashi[a,b], Roscoe O. Brady[c,2], and Yoshikatsu Eto[b]

Departments of [a]Gene Therapy and [b]Genetic Diseases and Genome Science, Jikei University School of Medicine, Tokyo 105-8461, Japan; and [c]National Institute of Neurological Disorders and Stroke, National Institutes of Health, Bethesda, MD 20892

Contributed by Roscoe O. Brady, March 5, 2010 (sent for review November 29, 2009)

Most lysosomal storage diseases (LSDs) are life-threatening genetic diseases. The pathogenesis of these diseases is poorly understood. Induced pluripotent stem (iPS) cell technology offers new opportunities for both mechanistic studies and development of stem cell–based therapies. Here we report the generation of disease-specific iPS cells from mouse models of Fabry disease, globoid cell leukodystrophy (GLD), and mucopolysaccharidosis VII (MPSVII). These mouse model–derived iPS cells showed defects in disease-specific enzyme activities and significant accumulation of substrates for these enzymes. In the lineage-directed differentiation studies, Fabry-iPS and GLD-iPS cells were efficiently differentiated into disease-relevant cell types, such as cardiomyocytes and neural stem cells, which might be useful in mechanistic and therapeutic studies. Notably, MPSVII-iPS cells demonstrated a markedly impaired ability to form embryoid bodies (EBs) in vitro. MPSVII-EBs exibited elevated levels of hyaluronan and its receptor CD44, and markedly reduced expression levels of E-cadherin and cell-proliferating marker. Partial correction of enzyme deficiency in MSPVII-iPS cells led to improved EB formation and reversal of aberrant protein expression. These data indicate a potential mechanism for the partial lethality of MPSVII mice in utero, and suggest a possible abnormality of embryonic development in MPSVII patients. Thus, our study demonstrates the unique promise of iPS cells for studying the pathogenesis and treatment of LSDs.

cardiomyocyte | embryoid body | neural stem cell

Lysosomal storage diseases (LSDs) are a group of life-threatening diseases with a global incidence of 1:7,000–8,000 live births (1, 2). Most LSDs are caused by deficiency of a single lysosomal enzyme or protein, which leads to abnormal accumulation of substrate in cells and subsequent cellular dysfunction. The pathogenesis of these diseases is poorly understood, however. For example, Fabry disease is associated with severe multisystem abnormalities including cardiac hypertrophy, progressive kidney disease, and stroke (3). The mechanism by which α-galactosidase A (α-gal A) deficiency and the resulting glycosphingolipid accumulation cause hypertrophy of myocytes is not known (4).

The paucity of mechanistic studies of LSDs is due largely to the absence of faithful in vitro disease model systems. Induced pluripotent stem (iPS) cells offer the opportunity to establish such in vitro models of LSDs, because iPS cells can be generated from skin fibroblasts of patients (5–7) and theoretically can differentiate into multiple cell types in vitro. In addition, the embryonic stem (ES) cell–like properties of iPS cells permit the study of early embryogenesis events in a culture system. This unique capability provides an invaluable tool for investigating that abnormal early embryonic development that may occur in these genetic disorders.

In addition, iPS cells provide a source for autologous cell transplantation, which may be useful to treat some LSDs. Enzyme replacement therapy (ERT) is a specific treatment for several LSDs (8, 9); however, systemic ERT is not effective for LSDs that affect the central nervous system, including globoid cell leukodystrophy (GLD) (10) and mucopolysaccharidosis (MPS) VII (11). For those LSDs, other strategies are needed to provide enzyme to the brain. Neural stem cell transplantation has been shown to improve neuropathology in mouse models with GLD and MPSVII (12–14). The use of iPS cell–derived neural stem cells or other cell types for transplantation might provide an attractive alternative to help overcome both donor shortages and immune rejection problems.

In the present study, we investigated the generation and characterization of iPS cells from mouse models of Fabry disease, GLD, and MPSVII. We also studied the relationship between β-glucuronidase (GUSB) deficiency and abnormal embryogenesis in vitro.

Results

Generation and Characterization of iPS Cells from Mouse Models. To generate iPS cells, we established primary cultures from tail-tip fibroblasts of mouse models of Fabry disease, GLD, and MPSVII, and of WT mice. Fibroblasts were infected with retroviruses encoding Oct3/4, Sox2, and Klf4 (15). iPS colonies were identified 1 week after being seeded on SNL feeder cells, and were ready for selection at 3 weeks. Generally, more than 10 clones from each model were isolated and expanded. Mouse iPS cells grew as colonies on top of feeder cells and had bright cytoplasm (Fig. 1*A*).

RT-PCR analysis showed that the putative iPS clones expressed ES cell marker genes. Almost all clones were positive for all 13 markers analyzed, including Nanog, Oct3/4, Ecat1, and Cripto (Fig. S1). Isolated clones were tested for expression of stage-specific embryonic antigen 1 (SSEA-1) and alkaline phosphatase (AP), undifferentiated cell markers identified by immunostaining and enzyme activity staining, respectively. All of the clones analyzed were strongly positive for SSEA-1 and AP (Fig. 1 *B* and *C*).

To examine whether these iPS cells are able to differentiate into multilineage cell types, cells were differentiated in vitro. Embryoid bodies (EBs) were formed after culturing in suspension for 3 days, then transferred to gelatin-coated dishes. After 3 days, differentiated cells were examined by immunostaining. Cells expressing β-tubulin III (ectoderm marker), α-fetoprotein (AFP; endoderm marker) and desmin (mesoderm marker) were detected, indicating that the iPS cells differentiated into cells of ectoderm, endoderm, and mesoderm lineages (Fig. S2).

The pluripotency of generated iPS cells was evaluated by teratoma formation. Between three and five clones of iPS cells of each mouse model were transplanted s.c. into nude mice. All formed tumors between 2 and 4 weeks after injection. Histological examination revealed neural tissue, muscle, cartilage, and respiratory epithelium–like tissue in the tumors (Fig. 2*A*). Immunostaining detected cells positive for β-tubulin III, GFAP, desmin,

Author contributions: X.-L.M., J.-S.S., and Y.E. designed research; X.-L.M., J.-S.S., S.K., and T.O. performed research; X.-L.M., J.-S.S., and R.O.B. analyzed data; and X.-L.M., J.-S.S., and R.O.B. wrote the paper.

The authors declare no conflict of interest.

[1]Present address: Institute of Metabolic Disease, Baylor Research Institute, Dallas, TX 75226.

[2]To whom correspondence may be addressed. E-mail: jinsong.shen@baylorhealth.edu or bradyr@ninds.nih.gov.

This article contains supporting information online at www.pnas.org/cgi/content/full/1002758107/DCSupplemental.

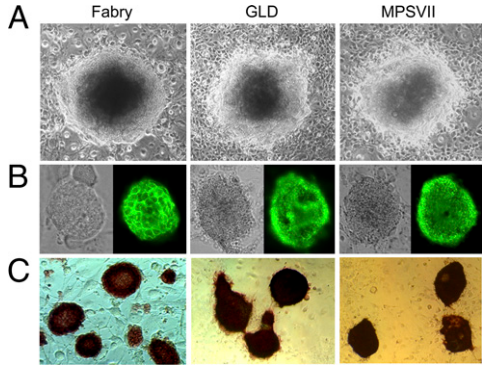

Fig. 1. Establishment of iPS cells from mouse models of Fabry, GLD, and MPSVII. Mouse iPS cells were established by retroviral transduction of Oct3/4, Sox2, and Klf4 into tail-tip fibroblasts. (*A*) iPS cells were grown on feeder cells and exhibited ES cell–like morphology. (*B* and *C*) All of the iPS clones analyzed were positive for SSEA1 (*B*, *Left*, phase contrast microscopy; *Right*, SSEA1 immunostaining) and alkaline phosphatase (*C*).

and AFP (Fig. 2*B*). Some rare cells were positive for the oligodendroglial marker GST-π (Fig. 2*B*). These results confirm that the mouse iPS cells differentiated into lineages for all three primary germ layers, and that they were pluripotent.

Disease phenotypes of the iPS cells were characterized. iPS cells from the LSD mouse models exhibited significantly reduced activities of the enzyme related to the specific disease compared with WT-iPS cells (Fig. 3*A*). Immunostaining for globotriaosylceramide (Gb3), the hallmark of Fabry disease, in undifferentiated Fabry-iPS cells revealed punctuate positive signals (Fig. 3*B*). No positive signals were detected in WT-iPS cells. Accumulation of Gb3 in Fabry-iPS cells was demonstrated by TLC (Fig. 3*C*). The content of hyaluronic acid (HA), the substrate of GUSB, was significantly higher in MPSVII-iPS-derived EBs (MPSVII-EBs) compared with WT- and Fabry-EBs (Fig. 3*D*).

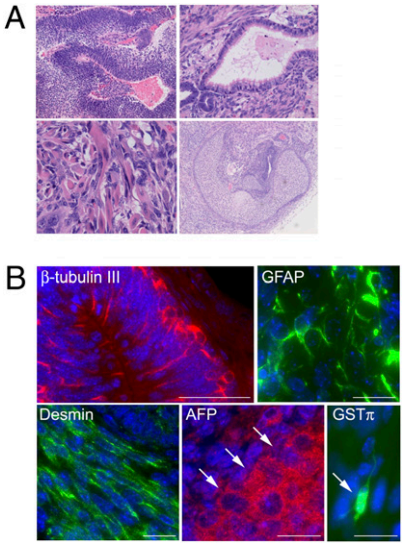

Fig. 2. In vivo analysis of pluripotency of disease-specific iPS cells. Pluripotency of the iPS cells was examined by teratoma formation. Histological and immunohistochemical analysis of tumors confirmed that iPS cells derived from three disease models were able to differentiate into all three germ layers. Representative data are shown. (*A*) Various tissues present in teratomas derived from Fabry-iPS: (*Left Upper*) Neural tissue. (*Right Upper*) Respiratory epithelium. (*Left Lower*) Muscle tissue. (*Right Lower*) Cartilage. (*B*) Immunostaining on Fabry-iPS–derived teratoma showing β-tubulin III$^+$ cells that formed cortical layer-like structures; GFAP$^+$ cells; desmin$^+$ cells with longitudinal cell bodies arrayed in parallel, and AFP$^+$ cells present as islets (arrows indicate the boundary of the islet). In addition to these markers, we also examined the ability of GLD-iPS cells to differentiate into oligodendrocytes. A few cells are positive for oligodendroglial marker GST-π, with typical morphology of type I oligodendrocytes (arrow). (Scale bars: 50 μm for β-tubulin III and 20 μm for GFAP, desmin, AFP, and GST-π).

Lineage-Directed Differentiation of the iPS Cells Into Disease-Relevant Cell Types. Lineage-directed differentiation of iPS cells into disease-relevant cell types in vitro is important for both mechanistic and therapeutic studies. Because cardiomyocytes are one of the major cell types affected in Fabry disease, we attempted to induce differentiation into cardiac cells. Fabry-iPS cells were cultured in suspension culture on low-attachment plates to allow formation of EBs. Between 6 and 7 days after attachment of the EBs onto gelatin-coated dishes, spontaneously beating areas were observed. The beating areas were dissected and reseeded on gelatin-coated dishes. Most reseeded cells demonstrated spontaneous beating as isolated single cells or cell clusters (Movie S1). On immunostaining, these beating cells were positive for cardiomyocyte markers, including actinin, cardiac troponin T, and GATA-4 (Fig. 4 *B–D*). Lysosomal accumulation of Gb3 also was confirmed in these differentiated Fabry cardiomyocytes (Fig. 4*E*).

The effect of the L-type calcium channel inhibitor diltiazem was studied on beating sites to determine whether the derived cardiomyocytes express the calcium channels required for initiation

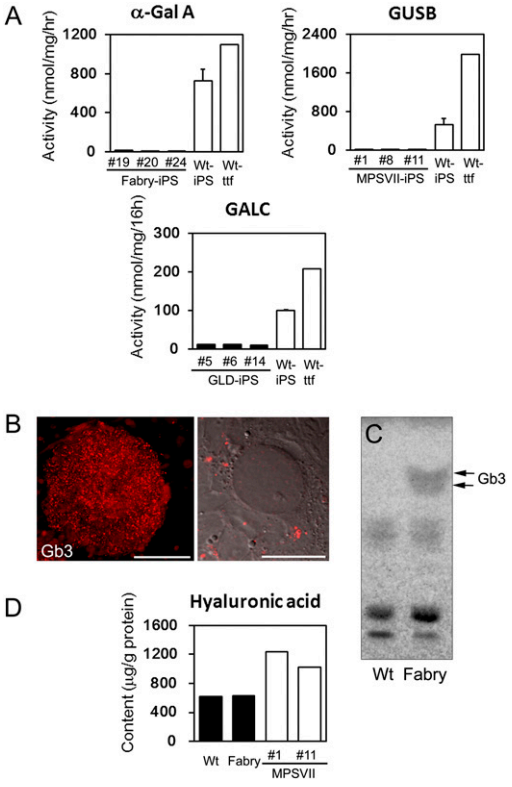

Fig. 3. Disease phenotype of mouse iPS cells. (*A*) Defects of specific enzyme activities in disease model–derived iPS cells were confirmed by enzyme assay. The numbers in the disease model–derived iPS are individual clone numbers. Data for iPS cells are presented as mean ± SD ($n = 3$). (*B*) Accumulated Gb3 in Fabry-iPS cells was confirmed by immunostaining. (*Left*) A colony of undifferentiated Fabry-iPS cells grown on the feeder cells is positive for Gb3. (*Right*) Confocal laser scanning microscopy confirmed positive signals in cytoplasm. [Scale bars: 200 μm (*Left*); 20 μm (*Right*).] (*C*) Analysis of Gb3 by TLC. (*D*) Elevated HA levels in EBs derived from MPSVII-iPS cells (two individual clones) was confirmed by HPLC.

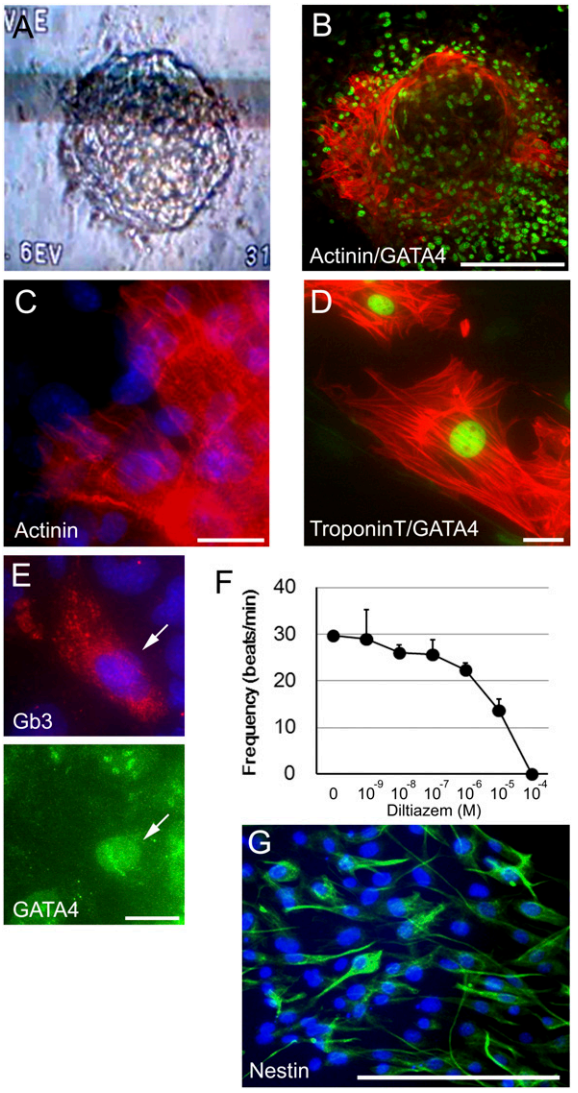

Fig. 4. Directed differentiation of iPS cells into disease-relevant cell types in vitro. (*A–F*) Directed differentiation of Fabry-iPS cells into cardiomyocytes. (*A*) Spontaneously beating cell clusters occurred after attachment of the EBs to gelatin-coated dishes. The photograph was printed from a video image showing a beating cell cluster. (*B*) Many cells in the cluster shown in *A* stained for cardiac cell markers actinin (red) and GATA-4 (green; nuclear localization). (*C* and *D*) Enlarged view of Fabry-iPS–derived cardiomyocytes expressing actinin (red) (*C*), Troponin T (red) and GATA-4 (green) (*D*). (*E*) Cardiomyocytes differentiated from Fabry-iPS cells exhibit accumulated Gb3 in the cytoplasm. (*Upper*) Gb3 staining (red). (*Lower*) GATA-4 staining (green, nuclear localization). (*F*) Effect of diltiazem, an L-type calcium channel blocker on the frequency of beating of Fabry-iPS–derived cardiomyocytes. Data are presented as mean ± SD ($n = 3$). (*G*) Differentiation to neural stem cells from GLD-iPS cells. After enrichment of neural stem cells, almost all of the differentiated cells were strongly positive for nestin. [Scale bars: 20 μm (*C–E*); 200 μm (*B* and *G*).]

of contractions in cardiac cells. The frequency of contractions was significantly decreased after diltiazem treatment, in a dose-dependent manner (Fig. 4*F*). These data conclusively demonstrate that Fabry disease cardiomyocytes can be generated from Fabry-iPS cells in vitro.

We also attempted to induce neural differentiation of GLD-iPS cells, because GLD abnormalities are limited almost exclusively to the nervous system. Through directed neuronal differentiation by EB formation in suspension culture and subsequent neural progenitor enrichment steps, we obtained a high-purity neural stem cell population. On immunostaining, almost all cells were strongly positive for the neural stem cell marker nestin (Fig. 4*G*).

Impaired EB Formation of MPSVII-iPS Cells. Our initial differentiation studies found that a significantly decreased capability for EB formation in MPSVII-iPS cells compared with WT-iPS cells and iPS cells from the other two disease models. Even though the same number of iPS cells were placed in suspension cultures, significantly fewer EBs were formed from MPSVII-iPS cells than from WT-iPS cells (Fig. 5*A*). In addition, the EBs formed from MPSVII-iPS cells generally were smaller than those formed from WT-iPS cells (Fig. 5*A*). Decreased efficiency of EB formation of MPSVII-iPS cells was seen as early as 24 h after dissociation and plating in suspension culture. The WT-EBs grew significantly larger by day 4, with few single cells seen at this time point. Although MPSVII-EBs also grew larger over time, many MPSVII-iPS cells remained as isolated single cells. This finding was consistent in several independent MPSVII-iPS clones and thus is not due to variations between individual clones. The EB formation from Fabry-iPS and GLD-iPS cells was indistinguishable from that from WT-iPS cells, suggesting that the defective EB formation is MPSVII-specific. To evaluate the efficiency of EB formation quantitatively, EBs larger than 100 μm (designated as EBs) and smaller than 100 μm (designated as filtrate) were separated by a cell strainer, and the cell numbers in each fraction were counted. Consistent with the microscopic findings described above, significantly fewer cells were counted in MPSVII-EBs compared with WT-, Fabry-, and GLD-EBs (Fig. 5*B*).

The decreased capability of MPSVII-iPS cells to form EBs was intriguing to us, because while maintaining a MPSVII mouse colony in our laboratory, we noted a much lower percentage of MPSVII newborns born from heterozygote mating than the expected 25% based on Mendelian inheritance (only 14.5%; 44 of 303 pups from 39 litters). This lower percentage of homozygotes was present before birth (20% at embryonic day 15–18; 11 of 55 fetuses from 6 litters). A similar finding (~18% of affected mice in both the prenatal and postnatal periods) was reported by another group (16). These observations suggest the possibility of intrauterine loss of some MPSVII embryos. Because in vitro EB recapitulates many aspects of the early stage of developing embryos (17, 18), the impaired EB formation of MPSVII-iPS might reflect aberrations in early embryogenesis in MPSVII mice that could lead to a partial loss of affected embryos.

We investigated the possible molecular basis for impaired EB formation of MPSVII-iPS cells. Because HA contributes to the migration and proliferation of the cells and plays important roles in mammalian embryogenesis (19), we speculated that the accumulation of HA might contribute to the EB abnormality. On HPLC analysis, MPSVII-EBs exhibited a 2-fold higher HA level compared with WT- and Fabry-EBs (Fig. 3*D*). We evaluated the expression of CD44, the main cell surface receptor for HA, by Western blot analysis and found significant increment of CD44 expression in MPSVII-EBs compared with WT- and Fabry-EBs (Fig. 5*C*).

The cell adhesion molecule E-cadherin plays a critical role in early embryogenesis and cell aggregation (20–22). A previous study reported an inverse correlation between HA expression and E-cadherin expression in keratinocytes (23). Based on our observation of decreased EB formation and elevated HA level in MPSVII-EBs, we hypothesized that E-cadherin expression might be down-regulated in MPSVII-EBs. Western blot analysis revealed markedly lower E-cadherin expression in MPSVII-EBs compared with WT- and Fabry-iPS EBs (Fig. 5*C*). This decreased E-cadherin expression in MPSVII-EBs was confirmed by immunofluorescence staining. In contrast to the strong positive signals in all cells in WT-EBs, only a few cells demonstrated weak signals in MPSVII-EBs (Fig. 5*D*).

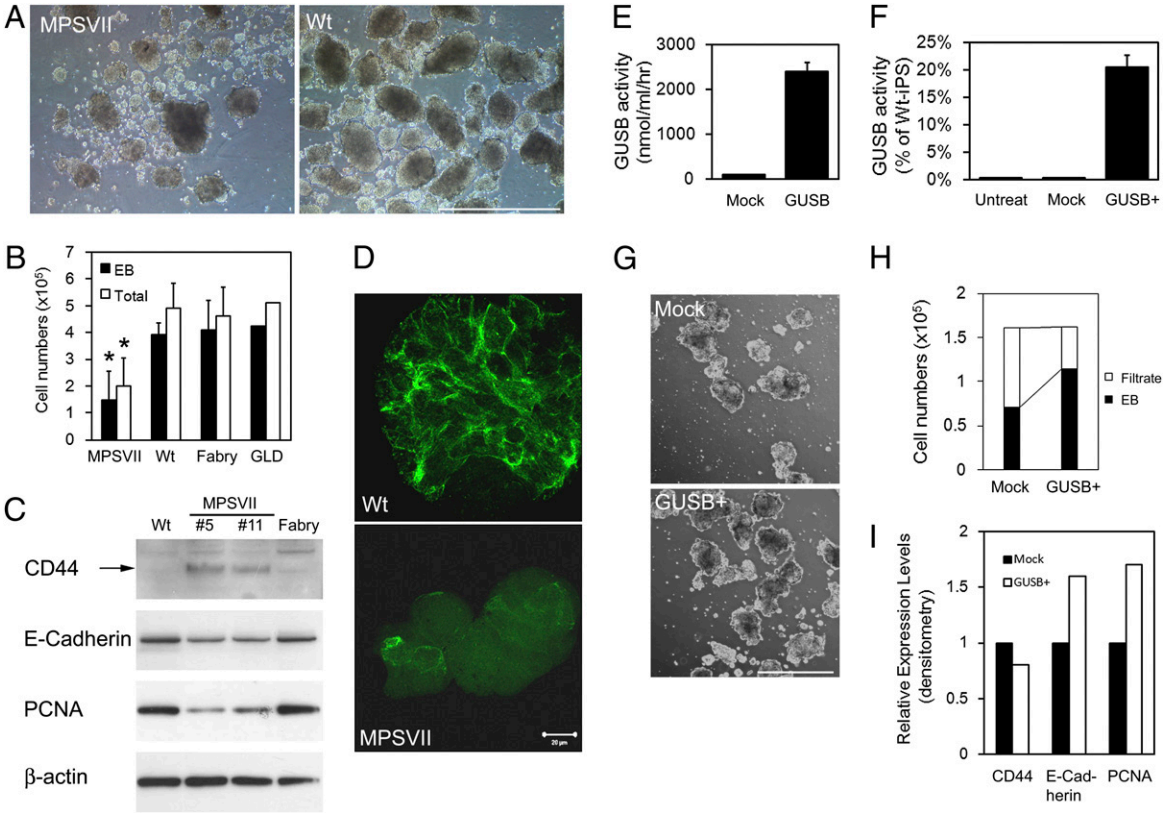

Fig. 5. Impaired EB formation of MPSVII-iPS cells. (*A*) Despite seeding the same number of cells, MPSVII-iPS cells formed significantly fewer and smaller EBs compared with WT-iPS cells. (*B*) EB formation was quantitated by counting cell numbers from dissociated EBs. The total cell number (sum of EB and filtrate fractions) is shown as well. Data for MPSVII-, WT-, and Fabry-EBs are presented as mean ± SD ($n = 3$). *$P < 0.05$, MPSVII-EBs compared with WT- and Fabry-EBs; two-tailed Student *t* test) (*C*) Western blot analysis revealed significantly increased expression of CD44 and decreased expression of E-cadherin and PCNA in MPSVII-EBs compared with Fabry- and WT-EBs. (*D*) Immunofluorescence staining (confocal laser microscopy) also confirmed markedly reduced expression of E-cadherin in MPSVII-EB compared with WT-EB. (*E–I*) MPSVII-iPS cells were treated with exogenous GUSB to determine whether the enzyme deficiency is the primary cause of impaired EB formation. (*E*) GUSB activity in conditioned media from 293T cells transfected with GUSB-expressing vector and a (mock) empty vector. (*F*) Uptake of GUSB in conditioned medium by MPSVII-iPS cells. (*G–I*) Enzyme treatment partially restored the efficiency of EB formation (*G* and *H*) and aberrant protein expression profile (*I*) of MPSVII-iPS. Data in *H* are means of three independent experiments. [Scale bars: 1 mm (*A*); 20 μm (*D*); 0.5 mm (*G*).]

To elucidate the direct causes of the decreased cell numbers in MPSVII-EBs, we evaluated cell proliferation and apoptosis. The cell proliferating marker proliferating cell nuclear antigen (PCNA) was expressed at a much lower level in MPSVII-iPS EBs than in WT- and Fabry-EBs (Fig. 5*C*); however, given that we did not detect activated caspase-3 in all samples, which would suggest programmed cell death, caspase-3–mediated cell death might not be significant at this stage of the EBs.

To confirm that the impaired EB formation and altered expression of CD44 and E-cadherin are due primarily to GUSB deficiency, we treated MPSVII-iPS cells with exogenous GUSB and analyzed the efficiency of EB formation. We used conditioned medium from GUSB overexpressing 293T cells as the enzyme source. After incubation with conditioned medium, the intracellular GUSB activity of the recipient MPSVII-iPS cells increased significantly (20% of WT-iPS cells), indicating efficient uptake of exogenous GUSB by these cells (Fig. 5*F*). For EB formation, MPSVII-iPS cells were fed with conditioned medium (with or without GUSB) for 3 days on feeder cells before differentiation. Subsequent suspension culture for EB formation also was carried out in the conditioned media with or without GUSB for 4 days. Enzyme treatment improved EB formation of MPSVII-iPS cells compared with MPSVII-iPS cells grown in conditioned medium without GUSB (Fig. 5 *G* and *H*). Enzyme treatment also led to lower CD44 expression and up-regulated expression of E-cadherin and PCNA (Fig. 5*I*).

Discussion

In this study, iPS cells generated from mouse models of Fabry disease, GLD, and MPSVII demonstrated defects in disease-specific enzymes and the accumulation of substrates of their enzymes. Fabry-iPS and GLD-iPS cells were efficiently differentiated into disease-relevant cell types in vitro. MPSVII-iPS cells exhibited a decreased ability to form EBs, suggesting possible abnormal embryogenesis in MPSVII.

One of the important potential applications of disease-specific iPS cells is to use in creating appropriate in vitro disease models. In this study, functional cardiomyocytes were efficiently differentiated from Fabry-iPS cells. This in vitro model could be used to examine potential links between the pathological accumulation of Gb3 or related glycosphingolipids, such as lyso-Gb3 (24), and cardiac hypertrophy–related substances, such as G protein, signaling kinases, and reactive oxygen species (25).

Previous studies have shown that transplantation of iPS cell–derived hematopoietic or neuronal stem cells can rescue disease phenotypes in murine models of sickle cell anemia and Parkinson's disease, respectively (26, 27). The effectiveness of iPS cells in treating LSDs remains to be demonstrated, however. Intrabrain transplantation of neural stem cells derived from GLD-iPS cells (after correction of the nonsense mutation in the GALC gene) into twitcher mice would provide a good model for elucidating the therapeutic potential of iPS cells in demyelinating disorders. Bone marrow transplantation has been reported to

result in significant clinicopathological improvement in multiple organs in MPSVII mice (28). Thus, investigations with iPS cell–derived hematopoietic stem cells might provide a model for evaluating the therapeutic potential of iPS cells in LSDs, in which many systems are affected.

An important feature of disease-specific iPS cells is that they can be used to study a disease at a very early stage of embryogenesis that is difficult or nearly impossible to study in vivo, especially in humans. One of the most interesting findings of the present study is the decreased capability of MPSVII-iPS cells to form EBs. Our observations suggest that the lower than expected percentage of MPSVII mice could have resulted from a loss of affected embryos during the implantation period and/or gestational period.

Decreased E-cadherin likely was a contributing factor to the decreased MPSVII-EB formation. E-cadherin plays a pivotal role in the compaction process of preimplantation embryos (20, 21). E-cadherin knockout embryos fail to form normal blastocysts and die around the time of implantation (21). Moreover, E-cadherin–null ES cells cannot form cell aggregates in suspension culture (22). The much smaller-sized aggregates formed by E-cadherin$^{+/-}$ ES cells compared with WT ES cells indicates that E-cadherin's effect on aggregate formation is dose-dependent. Despite the decreased EB formation, however, some of the MPSVII-EBs in our study grew to a substantial size and could be differentiated into all three germ layer cells. This partial defect in EB formation concurs with the observed partial lethality of MPSVII mice and likely is associated with reduced E-cadherin expression. An elevated HA level itself also might be involved in abnormal EB formation, because HA is thought to be required in many morphogenetic processes during development (19). Depletion of HA through disruption of its synthase (Has2) in mice was found to lead to serious cardiovascular defects and embryonic death at midgestation (29). Whether an elevated HA level has adverse effects in early embryogenesis is not known, however.

Our observations shed new light on the effect of defective lysosomal enzymes on embryogenesis in MPSVII and possibly other LSDs. Eventually, in vitro culture of the eggs collected from pregnant GUSB$^{+/-}$ mice will be needed to confirm a defect in early development in MPSVII and to study the underlying mechanism. Human iPS cells could be generated from MPSVII patients to examine whether this impaired EB formation exists in human iPS cells as well. Hydrops fetalis is known to be relatively common in patients with MPSVII (30). Further studies of iPS cells from human patients will help elucidate whether partial lethality also exists in human MPSVII embryos.

Materials and Methods

Mouse Models. Breeding pairs of twitcher heterozygotes (B6.CE-Galc^{twi}/J strain) and MPSVII heterozygotes (B6.C-*H2*^{bm1}/ByBir-*Gus*^{mps}/J strain) were purchased from Jackson Laboratory. Alpha-Gal A–deficient mice (31) were kindly provided by Dr. Ashok Kulkarni and Dr. Roscoe O. Brady (National Institutes of Health). The mouse colonies were maintained in our laboratory under standard housing conditions. All animal experiments were approved by Jikei University's Animal Experiments Committee.

Generation of iPS Cells. Mouse iPS cells were generated from fibroblasts using three transcription factors (Oct3/4, Sox2, and Klf4) according to the protocol described by Takahashi et al. (15). Tail biopsy specimens were obtained from each 5-month-old male Fabry mouse, 41-day-old female Twitcher mouse, 1 month-old female MPSVII mouse, and 2.5-month-old female normal C57BL/6J mouse. Primary cultures of tail-tip fibroblasts were obtained as described previously (15).

RT-PCR. Total RNA extraction and reverse-transcription reactions were performed as described previously (32), with primers and PCR conditions as described previously (15).

In Vitro Differentiation of iPS Cells. iPS cells were trypsinized and the cell suspensions were transferred to 100-mm Petri dishes at 1×10^6 cells per dish in ES medium (DMEM with 15% FBS, 2 mM L-glutamine, 0.1 mM nonessential amino acid, and 0.1 mM 2-mercaptoethanol). After 3 days, cell aggregates in the suspension culture were plated on gelatin-coated dishes in differentiation medium (Iscove's modified DMEM supplemented with 10% FBS, 2 mM glutamine, 0.1 mM nonessential amino acid, and 0.1 mM 2-mercaptoethanol). After 3 days, the cells were stained with antibodies against cell type–specific markers.

Teratoma Formation Study. Approximately 1×10^6 cells in 100 μL were injected s.c. to the dorsal flank of nude mice. After 2–4 weeks, tumors were dissected, fixed in 10% formaldehyde in phosphate buffer, and embedded in paraffin. Then 4-μm sections were stained with hematoxylin and eosin or used for immunostaining.

Immunostaining and Alkaline Phosphatase Staining. See *SI Materials and Methods*.

Embryoid Body Formation and Its Efficiency. Undifferentiated iPS cells on feeder cells were trypsinized, and the cell suspensions were plated onto tissue culture dishes for 1 h at 37 °C to allow feeder cells to attach to the dish. The unattached iPS cells were collected and plated on ultra–low attachment six-well plates (Corning) at 1.5×10^5 cells per well in the aforementioned differentiation medium to initiate EB formation. The efficiency of EB formation was determined as described previously, with modifications (33). In brief, suspension cultures of EBs were passed through a 100-μm cell strainer, and the filtrates were collected. The cell strainer with trapped EBs was decanted into a 50-mL tube and washed thoroughly with PBS to collect EBs. Two fractions (EBs and filtrates) were dissociated with 0.25% trypsin-EDTA, and cell numbers were counted.

Cardiomyocyte and Neural Stem Cell Differentiation. Lineage-directed differentiation of iPS cells into cardiomyocytes and neural stem cells was induced through EB formation suspension culture and subsequent attachment (*SI Materials and Methods*).

Lysosomal Enzyme Assays. Activities of α-gal A and GUSB were determined by 4-methylumbellferyl–labeled substrates as described previously (34, 35). Activity of β-galactocerebrosidase was determined by fluorometric assay using 6-hexadecanoylamino-4-methylumbelliferyl-β-D-galactoside as a substrate, as described previously (36), with modifications (see *SI Materials and Methods* for details).

TLC. Lipid extraction and TLC was performed as described previously (32), except that silica gel high-performance TLC plates (Merck) were used, and the spots were visualized by 50% sulfuric acid.

HPLC Analysis of Hyaluronic Acid. Cell lysates were subjected to enzyme digestion and HPLC procedures as described previously (13).

Western Blot Analysis. Western blot analysis was performed as described previously (32) (see *SI Materials and Methods* for details). The relative expression levels of the proteins were determined by densitometry using NIH Image software.

GUSB Enzyme Treatment. 293T cells were transfected with a vector expressing human β-glucuronidase (pLHCHBG) (13) or empty vector (pLHCX) using Lipofectamine 2000 (Invitrogen) according to the manufacturer's recommendations. The pilot study demonstrated that in this expression system, GUSB was expressed at very high levels at 2–7 days after transfection, and that a large amount of the enzyme was secreted into the medium. Two-day-old conditioned medium (with or without GUSB) was mixed with an equal volume of fresh medium and used to feed MPSVII cells. Undifferentiated MPSVII-iPS cells were incubated in this enzyme-containing ES medium for 3 days before EB formation. Then EB formation was initiated and maintained in suspension culture as described above in enzyme-containing differentiation medium for 4 days or until analysis.

ACKNOWLEDGMENTS. We thank Dr. Toshio Kitamura (University of Tokyo) for providing the Plat-E packaging cell line (37), Y. Kurahashi (Seikagaku Corp) for performing the HPLC analysis of hyaluronan, and E. Kikuchi (Jikei University) for helping with the confocal laser microscopy. We also thank Dr. Raphael Schiffmann (Institute of Metabolic Disease, Baylor Research Institute) for comments on and critical editing of the manuscript. This work was supported by the Jikei University Research Fund, a Grant-in-Aid for Young Scientists from the Japan Society for the Promotion of Science, and a Grant for Research for Intractable Diseases from the Japanese Ministry of Health, Welfare, and Labor.

1. Meikle PJ, Hopwood JJ, Clague AE, Carey WF (1999) Prevalence of lysosomal storage disorders. *JAMA* 281:249–254.
2. Poorthuis BJ, et al. (1999) The frequency of lysosomal storage diseases in The Netherlands. *Hum Genet* 105:151–156.
3. Desnick RJ, Ioannou YA, Eng CM (2001) a-Galactosidase A deficiency: Fabry disease. *The Metabolic and Molecular Bases of Inherited Disease*, eds Scriver CR, Beaudet AL, Sly WS, Valle D (McGraw-Hill, New York), 8th Ed, Vol 3, pp 3733–3774.
4. Schiffmann R (2009) Fabry disease. *Pharmacol Ther* 122:65–77.
5. Takahashi K, Yamanaka S (2006) Induction of pluripotent stem cells from mouse embryonic and adult fibroblast cultures by defined factors. *Cell* 126:663–676.
6. Takahashi K, et al. (2007) Induction of pluripotent stem cells from adult human fibroblasts by defined factors. *Cell* 131:861–872.
7. Nakagawa M, et al. (2008) Generation of induced pluripotent stem cells without Myc from mouse and human fibroblasts. *Nat Biotechnol* 26:101–106.
8. Brady RO (2006) Enzyme replacement for lysosomal diseases. *Annu Rev Med* 57: 283–296.
9. Desnick RJ (2004) Enzyme replacement and enhancement therapies for lysosomal diseases. *J Inherit Metab Dis* 27:385–410.
10. Wenger DA, Suzuki K, Suzuki Y, Suzuki K (2001) Galactosylceramide lipidosis: Globoid cell leukodystrophy (Krabbe disease). *The Metabolic and Molecular Bases of Inherited Disease*, eds Scriver CR, Beaudet AL, Sly WS, Valle D (McGraw-Hill, New York), 8th Ed, Vol 3, pp 3669–3694.
11. Sly WS, Quinton BA, McAlister WH, Rimoin DL (1973) Beta glucuronidase deficiency: Report of clinical, radiologic, and biochemical features of a new mucopolysaccharidosis. *J Pediatr* 82:249–257.
12. Snyder EY, Taylor RM, Wolfe JH (1995) Neural progenitor cell engraftment corrects lysosomal storage throughout the MPS VII mouse brain. *Nature* 374:367–370.
13. Meng XL, et al. (2003) Brain transplantation of genetically engineered human neural stem cells globally corrects brain lesions in the mucopolysaccharidosis type VII mouse. *J Neurosci Res* 74:266–277.
14. Strazza M, et al. (2009) Significant correction of pathology in brains of twitcher mice following injection of genetically modified mouse neural progenitor cells. *Mol Genet Metab* 97:27–34.
15. Takahashi K, Okita K, Nakagawa M, Yamanaka S (2007) Induction of pluripotent stem cells from fibroblast cultures. *Nat Protoc* 2:3081–3089.
16. Casal ML, Wolfe JH (2000) Mucopolysaccharidosis type VII in the developing mouse fetus. *Pediatr Res* 47:750–756.
17. Keller GM (1995) In vitro differentiation of embryonic stem cells. *Curr Opin Cell Biol* 7: 862–869.
18. Coucouvanis E, Martin GR (1995) Signals for death and survival: A two-step mechanism for cavitation in the vertebrate embryo. *Cell* 83:279–287.
19. Spicer AP, Tien JY (2004) Hyaluronan and morphogenesis. *Birth Defects Res C Embryo Today* 72:89–108.
20. Hyafil F, Morello D, Babinet C, Jacob F (1980) A cell surface glycoprotein involved in the compaction of embryonal carcinoma cells and cleavage stage embryos. *Cell* 21: 927–934.
21. Larue L, Ohsugi M, Hirchenhain J, Kemler R (1994) E-cadherin null mutant embryos fail to form a trophectoderm epithelium. *Proc Natl Acad Sci USA* 91:8263–8267.
22. Fok EY, Zandstra PW (2005) Shear-controlled single-step mouse embryonic stem cell expansion and embryoid body-based differentiation. *Stem Cells* 23:1333–1342.
23. Ohtani T, et al. (2009) Increased hyaluronan production and decreased E-cadherin expression by cytokine-stimulated keratinocytes lead to spongiosis formation. *J Invest Dermatol* 129:1412–1420.
24. Aerts JM, et al. (2008) Elevated globotriaosylsphingosine is a hallmark of Fabry disease. *Proc Natl Acad Sci USA* 105:2812–2817.
25. Gupta S, Das B, Sen S (2007) Cardiac hypertrophy: Mechanisms and therapeutic opportunities. *Antioxid Redox Signal* 9:623–652.
26. Hanna J, et al. (2007) Treatment of sickle cell anemia mouse model with iPS cells generated from autologous skin. *Science* 318:1920–1923.
27. Wernig M, et al. (2008) Neurons derived from reprogrammed fibroblasts functionally integrate into the fetal brain and improve symptoms of rats with Parkinson's disease. *Proc Natl Acad Sci USA* 105:5856–5861.
28. Sands MS, et al. (1993) Treatment of murine mucopolysaccharidosis type VII by syngeneic bone marrow transplantation in neonates. *Lab Invest* 68:676–686.
29. Camenisch TD, et al. (2000) Disruption of hyaluronan synthase-2 abrogates normal cardiac morphogenesis and hyaluronan-mediated transformation of epithelium to mesenchyme. *J Clin Invest* 106:349–360.
30. Nelson A, Peterson L, Frampton B, Sly WS (1982) Mucopolysaccharidosis VII (beta-glucuronidase deficiency) presenting as nonimmune hydrops fetalis. *J Pediatr* 101: 574–576.
31. Ohshima T, et al. (1997) alpha-Galactosidase A–deficient mice: A model of Fabry disease. *Proc Natl Acad Sci USA* 94:2540–2544.
32. Shen JS, et al. (2008) Globotriaosylceramide induces oxidative stress and up-regulates cell adhesion molecule expression in Fabry disease endothelial cells. *Mol Genet Metab* 95:163–168.
33. Carpenedo RL, Sargent CY, McDevitt TC (2007) Rotary suspension culture enhances the efficiency, yield, and homogeneity of embryoid body differentiation. *Stem Cells* 25:2224–2234.
34. Kusiak JW, Quirk JM, Brady RO (1978) Purification and properties of the two major isozymes of alpha-galactosidase from human placenta. *J Biol Chem* 253:184–190.
35. Glaser JH, Sly WS (1973) Beta-glucuronidase deficiency mucopolysaccharidosis: Methods for enzymatic diagnosis. *J Lab Clin Med* 82:969–977.
36. Wiederschain G, Raghavan S, Kolodny E (1992) Characterization of 6-hexadecanoylamino-4-methylumbelliferyl-beta-D- galactopyranoside as fluorogenic substrate of galacto-cerebrosidase for the diagnosis of Krabbe disease. *Clin Chim Acta* 205:87–96.
37. Morita S, Kojima T, Kitamura T (2000) Plat-E: An efficient and stable system for transient packaging of retroviruses. *Gene Ther* 7:1063–1066.